NASA Contractor Report 185253

Nonlinear Structural Analysis of Cylindrical Thrust Chambers Using Viscoplastic Models

Vinod K. Arya
University of Toledo
Toledo, Ohio

January 1991

NASA
National Aeronautics and
Space Administration

NONLINEAR STRUCTURAL ANALYSIS OF CYLINDRICAL THRUST CHAMBERS USING VISCOPLASTIC MODELS

Vinod K. Arya
University of Toledo
Toledo, Ohio 43606

Summary

Elevated temperature and pressure levels are required for improving the performance of the Space Shuttle Main Engine (SSME). At these elevated temperatures, the thrust chamber of the engine experiences significant inelastic strains. For an accurate estimation of the life of the chambers and to predict their progressive deformation with the number of loading cycles, a realistic stress-strain analysis for the components must be made.

This paper presents the results of a viscoplastic stress-strain analysis of a cylindrical thrust chamber used in experiments at the NASA Lewis Research Center. The experiments were designed to simulate the SSME operating conditions. The inelastic strain was calculated by using a viscoplastic model developed by Freed, and the quasi-three-dimensional structural analysis was performed by using the finite element program MARC. The temperatures and pressures were calculated by using the loading cycles of experiments, and these temperatures and pressures were used in the computations. The deformed shape of the component was predicted after the end of each loading cycle. The predicted shape qualitatively replicated the deformed shape of the component as observed in experiments. The results indicate that the use of viscoplastic models for structural analysis may lead to more realistic life assessments of experimental thrust chambers.

Introduction

High performance, reusability, compact size, and light weight are requirements for the Space Shuttle Main Engine (SSME). Elevated temperature and pressure levels, and thrust chamber materials capable of withstanding a large number of loading cycles, high strain levels, and high heat fluxes are necessary to meet these requirements. At such temperatures, the cylindrical thrust chambers of the rocket engine experience significant inelastic strains. Furthermore, at these high temperatures, an interaction between plasticity (time-independent, inelastic strain) and creep (time-dependent, inelastic strain) is observed. Therefore, for an accurate estimation of the life of thrust chambers, a realistic, inelastic stress-strain analysis is required. This analysis must include the effects of observed creep and plasticity interactions. Conventional inelastic analyses of structural components treat the plastic and creep strains as independent, noninteracting entities and are, therefore, inadequate for such applications.

Owing to the high costs and other considerations associated with the analysis of the SSME thrust chamber, a simplified cylindrical thrust chamber assembly was employed in the experiments performed at the NASA Lewis Research Center, (ref. 1). These experiments were designed to simulate the operating conditions experienced by the SSME. A schematic, taken from reference 1, and a photograph of the cylindrical thrust chamber assembly used in these experiments are shown in figure 1. The thrust chamber consists of an annular injector, a liquid-hydrogen-cooled outer cylinder, and a water-cooled centerbody that forms the annular thrust chamber throat. The pressure, thrust, and average throat heat flux in the chamber were 4.14 MN/m^2 (600 psia), 5.34 kN (1200 lbf), and 54 MW/m^2 (33 Btu/in.^{2}/sec), respectively. Further details of experiments and apparatus can be found in references 1 and 2.

A cross section of the cylinder wall with cooling channel dimensions is shown in figure 2. The cylinder wall contains 72 cooling channels. The shaded area in this figure depicts the segment of the component modeled for the thermal and structural analyses. Table I shows the cyclic thermal and pressure loadings in the chamber taken from ref. 3. These cyclic thermomechanical loadings imposed on the cylindrical chambers progressively deformed the cooling channels and cooling passage walls, resulting in the "dog house" effect seen in the experiments of reference 1 and shown in figure 3. The
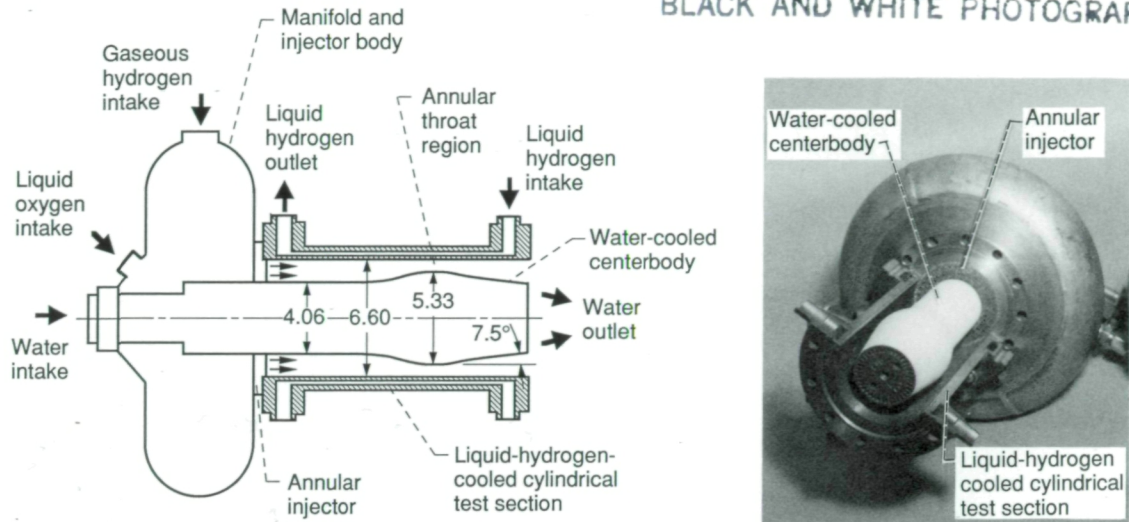
Figure 1.—Annular rocket thrust chamber assembly (from ref. 1). All dimensions in centimeters unless indicated otherwise.
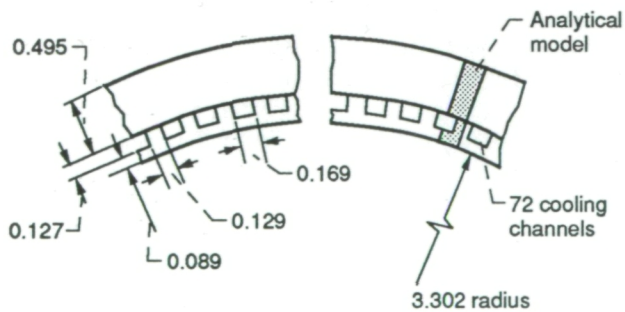

Figure 2.—Cylinder wall cross section showing the analytical model and dimensions (from ref. 2). All dimensions in centimeters.
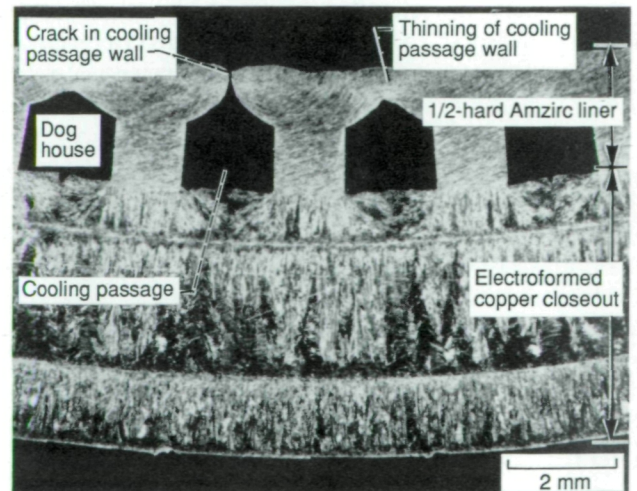

Figure 3.—Cross section of ½-hard Amzirc cylinder at the throat plane after 393 thermal cycles (from ref. 1).

TABLE I.—CYCLIC TEMPERATURE AND PRESSURE LOADING HISTORIES
[From ref. 3.]

	Cold phase	Hot phase
Hot-gas-side heat transfer coefficient, W/cm^2-K (Btu/in.^{2}-sec-R)	0	2.02 (0.00685)
Hot-gas-side adiabatic wall temperature, K (°R)	278 (500)	3364 (6055)
Hot-gas-side wall pressure, kN/m^2 (psia)	96.5 (14.0)	2780 (403)
Coolant-side heat transfer coefficient, W/cm^2-K (Btu/in.^{2}-sec-R)	10.2 (0.0345)	4.83 (0.0164)
Coolant-side bulk temperature, K (°R)	28 (50)	50 (90)
Coolant-side wall pressure, kN/m^2 (psia)	5100 (740)	6550 (950)

Typical Cycle History
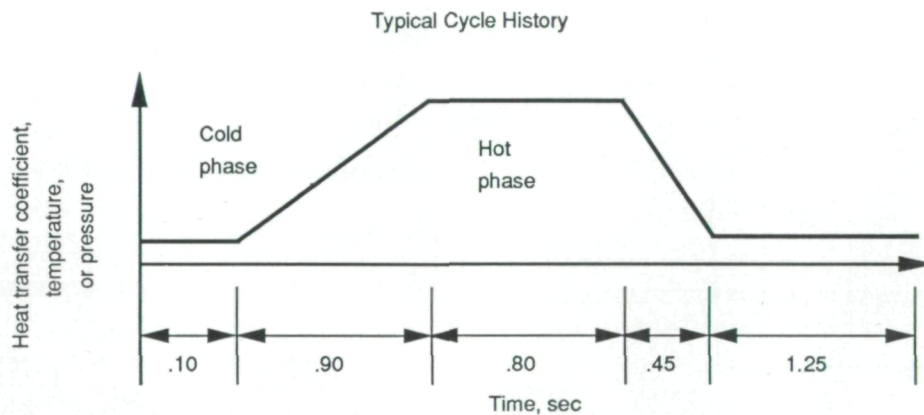
failure of the component is characterized by thinning of the cooling channel wall and its eventual failure by tensile rupture (fig. 4). Therefore, for accurate predictions of the progressive deformation of the wall and channels (leading to the "dog house" effect) and for predictions of the thrust chamber's service life under cyclic thermomechanical loadings, a realistic stress-strain analysis must be performed.

During the last two decades or so, a number of constitutive models, called viscoplastic models, have been proposed to describe the high-temperature, time-dependent, inelastic behavior of materials. The observed interactions among the inelastic strains (creep, plastic, relaxation, etc.) are included in these models by treating all the inelastic strains as a single time-dependent quantity. Viscoplastic models provide realistic descriptions of high-temperature inelastic behavior of materials and thus facilitate realistic, inelastic stress-strain analysis. The mathematical structure of these models is, however, very com-

plicated. Furthermore, complex thermomechanical loadings and complex geometries associated with the majority of structural engineering problems, such as cylindrical thrust chambers, make closed-form solutions virtually impossible. Therefore, the stress-strain analysis for such problems requires numerical methods such as the finite element method or the boundary element method.

In the present study, a finite element stress-strain analysis of a cylindrical thrust chamber nozzle (which was used in the ref. 1 experiments) was performed. The inelastic strains in the nozzle were computed by using a unified viscoplastic constitutive model developed by Freed (ref. 4). The thermomechanical loading cycles of the experiments were used in the calculations. The nonlinear variations in temperature-dependent material properties were accounted for in the computations as well. The next section presents a brief description of Freed's viscoplastic model.
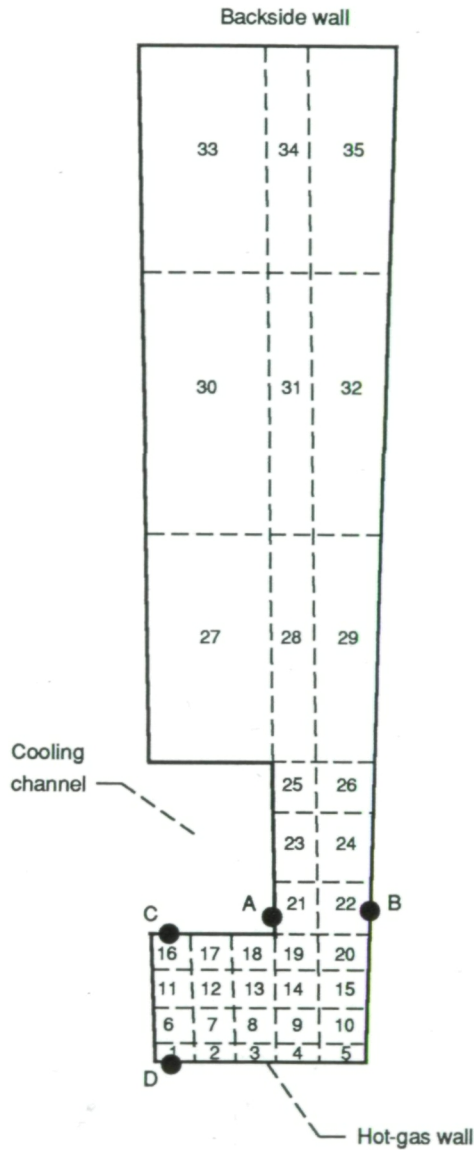
Figure 4.—Finite element model for cylindrical thrust chamber; 35 elements, 54 nodes.

thermal $\dot{\varepsilon}_{ij}^{th}$ strain-rate components. This decomposition can be shown as

$$\dot{\varepsilon}_{ij} = \dot{\varepsilon}_{ij}^{el} + \dot{\varepsilon}_{ij}^{in} + \dot{\varepsilon}_{ij}^{th} \qquad (i,j = 1,2,3) \qquad (1)$$

The elastic strain-rate is governed by Hooke's law:

$$\dot{\varepsilon}_{ij}^{el} = \frac{1 + \nu}{E}\,\dot{\sigma}_{ij} - \frac{\nu}{E}\,\dot{\sigma}_{kk}\delta_{ij} \qquad (2)$$

where E is the Young's modulus, ν is the Poisson's ratio, and σ_{ij} is the stress. The repeated subscripts in equation (2) and elsewhere imply summation over their range, and δ_{ij} is the Kronecker delta function. A dot over a symbol denotes its derivative with respect to time t.

Defining the deviatoric stress S_{ij} by

$$S_{ij} = \sigma_{ij} - \frac{1}{3}\,\sigma_{kk}\,\delta_{ij} \qquad (3)$$

and the effective stress Σ_{ij} by

$$\Sigma_{ij} = S_{ij} - B_{ij} \qquad (4)$$

yields the following flow and evolutionary laws for the model:

Flow Law

$$\dot{\varepsilon}_{ij}^{in} = \Theta Z \frac{\Sigma_{ij}}{J_2} \qquad (5)$$

where

$$J_2 = \frac{1}{2}\,\Sigma_{ij}\Sigma_{ij} \qquad (6)$$

The thermal-diffusivity function Θ contains the temperature dependence of the model and is defined by

$$\Theta = \begin{cases} \exp(-Q/kT) & T \geq 0.5\ T_m \\[2ex] \exp\left\{\dfrac{-2Q}{kT_m}\left[\ln\left(\dfrac{T_m}{2T}\right) + 1\right]\right\} & T \leq 0.5\ T_m \end{cases} \qquad (7)$$

where Q is the activation energy, k is the Boltzmann constant, T is the absolute temperature, and T_m is the melting point of the material.

Freed's Viscoplastic Model

In keeping with the general mathematical structure of viscoplastic models, the viscoplasticity effects in Freed's model are incorporated through two types of internal state variables— a tensorial back stress B_{ij} and a drag stress D. The back stress accounts for kinematic, or flow-induced, anisotropic hardening, whereas the drag stress accounts for isotropic hardening. The static and dynamic recovery terms in the model are assumed to be uncoupled. This yields a simpler mathematical framework for the model.

The total strain rate $\dot{\varepsilon}_{ij}$ is decomposed into elastic $\dot{\varepsilon}_{ij}^{el}$, inelastic $\dot{\varepsilon}_{ij}^{in}$ (including plastic, creep, and relaxation), and

The function Z, called the Zener-Hollomon parameter, is defined by

$$Z = \begin{cases} AF^n & F \le 1 \\ A \exp[n(F-1)] & F \ge 1 \end{cases} \tag{8}$$

where A and n are material constants, and the function F is defined as

$$F = \frac{J_2}{D} \tag{9}$$

Here D denotes the drag stress.

Evolutionary Laws

The differential equations governing the growth of the internal state variables, that is, the back stress B_{ij} and the drag stress D are

$$\dot{B}_{ij} = H\left(\dot{\varepsilon}_{ij}^{in} - \frac{B_{ij}}{L} I_2\right) \tag{10}$$

and

$$\dot{D} = h\left(\frac{I_2}{G} - \Theta r(G)\right) \tag{11}$$

where

$$I_2 = \Theta Z$$

In the above equations h, H, and L are inelastic material constants. The constant L is the limiting value of the back stress at kinematic saturation (ref. 4). The recovery function r is defined through the following equations:

$$r(G) = \begin{cases} 0 & D = D_o \\ R(G) & D > D_o \end{cases} \tag{12}$$

and

$$R(G) = \begin{cases} AG^{n-1} & G \le 1 \\ A \exp\left[\frac{n(G-1)}{G}\right] \ge 1 \end{cases} \tag{13}$$

and

$$G = \frac{L}{S - D} \tag{14}$$

TABLE II.—MATERIAL CONSTANTS FOR COPPER[a]
[From ref. 1.]

Young's modulus, E, MPa	$165\,000 - 125T$
α, °C^{-1}	$15 \times 10^{-6} + 5 \times 10^{-9}T$
Poisson's ratio, ν	0.34
A, sec^{-1}	50 000 000
D_o, MPa	1.5
Inelastic material constant, h, MPa	500
Inelastic material constant, H, MPa	5000
Limiting value of back stress at kinematic saturation, L, MPa	$25 \exp(-T/300)$
n	5
Activation energy, Q, J/mole	200 000
S, MPa	14.3
Melting point, T_m, K	1356

[a]T is absolute temperature in degrees centigrade.

where S and D_o are material constants.

Furthermore, satisfying the dissipativity condition yields the following constraint for the function r

$$r \ge Z\left[\frac{1}{G} - 2F + \frac{B_2^2}{LD}\right] \tag{15}$$

in which

$$B_2 = \frac{1}{2} B_{ij} B_{ij} \tag{16}$$

This condition must be satisfied for the theory to be thermo-dynamically admissible. The material of the cylindrical nozzle is assumed to be copper. The values of material constants for copper (taken from ref. 4) are listed in table II.

Analyses

This section provides the details of the finite element model, thermal analysis, and stress analysis.

Finite Element Model

The finite element model used for thermal and stress analyses is shown in figure 4. Because of symmetry, only one-half of a cooling channel was modeled. Generalized plane-strain, isoparametric elements were used to model this smallest repeating segment of the cylinder wall, thereby facilitating a quasi-three-dimensional analysis. The finite element model consisted of 35 elements and 54 nodes.

Thermal Analysis

A thermal analysis to generate the cross-sectional temperature was performed by Quentmeyer (ref. 1). The

5

thermal analyzer program SINDA (ref. 5) was used to perform the thermal analysis. Time-dependent hot-gas-side and coolant-side boundary conditions were input to the SINDA program to obtain the temperature profile as a function of time. Some assumptions and approximations were made in the thermal analysis to estimate the quantities for which no experimental data were available. Complete details of the thermal analysis can be found in reference 1.

Finite Element Analysis

The highly nonlinear and mathematically "stiff" nature of the constitutive equations of viscoplastic models requires the development and application of suitable numerical solution technologies involving, for example, the finite element method. For efficient and accurate time integration of the constitutive equations, special time-integration strategies are required. A numerical solution technology employing the finite element program MARC (ref. 6) was used for the stress analysis of the cylindrical chambers. The details of this finite-element-based solution technology may be found in Arya and Kaufman (ref. 7), and Arya (ref. 8). A self-adaptive integration strategy utilizing the explicit forward Euler method developed by Arya et al. (ref. 9) is employed for the time integration of the constitutive equations of the model. The integration strategy is easy to use, and works well even for problems with complex geometries and loadings (Arya, refs. 10 and 11).

The time-dependent temperature distribution obtained from the thermal analysis described in the preceding section was utilized to perform the finite element thermostructural analysis. Elemental pressure loadings and time-varying nodal temperatures were applied to trace the loading cycles of table I. The nonlinear variations in the temperature-dependent material properties were accounted for in the computations.

Results and Discussion

Several uniaxial problems involving the isothermal and nonisothermal (both inphase and out-of-phase) loadings were analyzed in reference 10 to validate the finite element implementation of Freed's model. The results obtained by using the implementation showed good agreement with the experimental results, implying correct finite element implementation of the model. This "validated" implementation was used to perform the stress-strain analysis for the cylindrical thrust chamber nozzle problem.

The circumferential (x-direction) stress distributions in the nozzle at the completion of the first and fifth loading cycles of figure 2 are shown in figure 5. The stresses are tensile throughout the segment of the component used for the finite element analysis. At the end of the first cycle the maximum circumferential stress occurred in the lower part of the component. This maximum stress relaxed and redistributed with

the loading cycles. Relaxation is indicated by a considerable reduction of the stress (after the fifth cycle) in the lower part of the segment. The stress increases in the upper part of the segment (fig. 5(b)). Figure 6 exhibits the radial (y-direction) stress distribution in the nozzle at the end of the first and fifth loading cycles. A redistribution of stress similar to that for the circumferential stress is observed for the radial stress also. The effective stress distribution in the segment at the end of the first and fifth loading cycles is shown in figure 7. The effective stress is redistributed in a way similar to that observed for the circumferential and radial stresses.

The circumferential (x-direction) strain distribution in the segment is shown in figure 8. The strain values, plotted after the end of the first and fifth loading cycles in this figure (and elsewhere), are the sum of mechanical and thermal strains. There is almost no redistribution of the circumferential strain in the upper part of the segment with successive loading cycles. The circumferential strain in the lower part of the segment increases in magnitude everywhere except at a few points. This increase in circumferential strain magnitude is substantial at some locations.

Figure 9 shows the radial (y-direction) strain distribution after the end of the first and fifth loading cycles. Not much change in the strain values is observed in the upper part of the component. However, in general, in the lower part of the component the strain increases considerably in magnitude with the number of cycles. The radial compressive strain increases in magnitude and propagates from the lower left corner of the coolant channel into the channel wall. The tensile strains also increase in magnitude in the lower part of the segment.

The displacements in the circumferential direction (x-direction) versus loading cycles at point A on the cooling channel wall (fig. 4) are shown in figure 10. The displacements increase in magnitude with the number of loading cycles. Since the corresponding point B on the segment wall (fig. 4) is constrained in the x-direction, the wall thickness decreases with the increasing number of loading cycles.

The displacements in the radial direction (y-direction) are plotted in figure 11 at point C on the cooling channel wall (fig. 4) versus the number of cycles. The displacement values plotted are the values at the end of the corresponding loading cycle. The absolute value of the displacement increases with the number of cycles. This implies that the channel cross-section will deform progressively, leading to the "dog house" effect observed in experiments (see fig. 3). Figure 11 also shows displacements in the radial direction (y-direction) at point D on the hot-gas chamber wall (fig. 4). This point is situated in the same vertical plane as the point C, and it corresponds to the lowest point on the channel wall. A comparison of the displacement curves for these two points reveals that the displacements at point C are larger than the corresponding displacements at point D. This means that the coolant channel wall diminishes in thickness with each loading cycle. The present analysis is thus capable of explaining the thinning of the coolant channel that was observed in experiments.
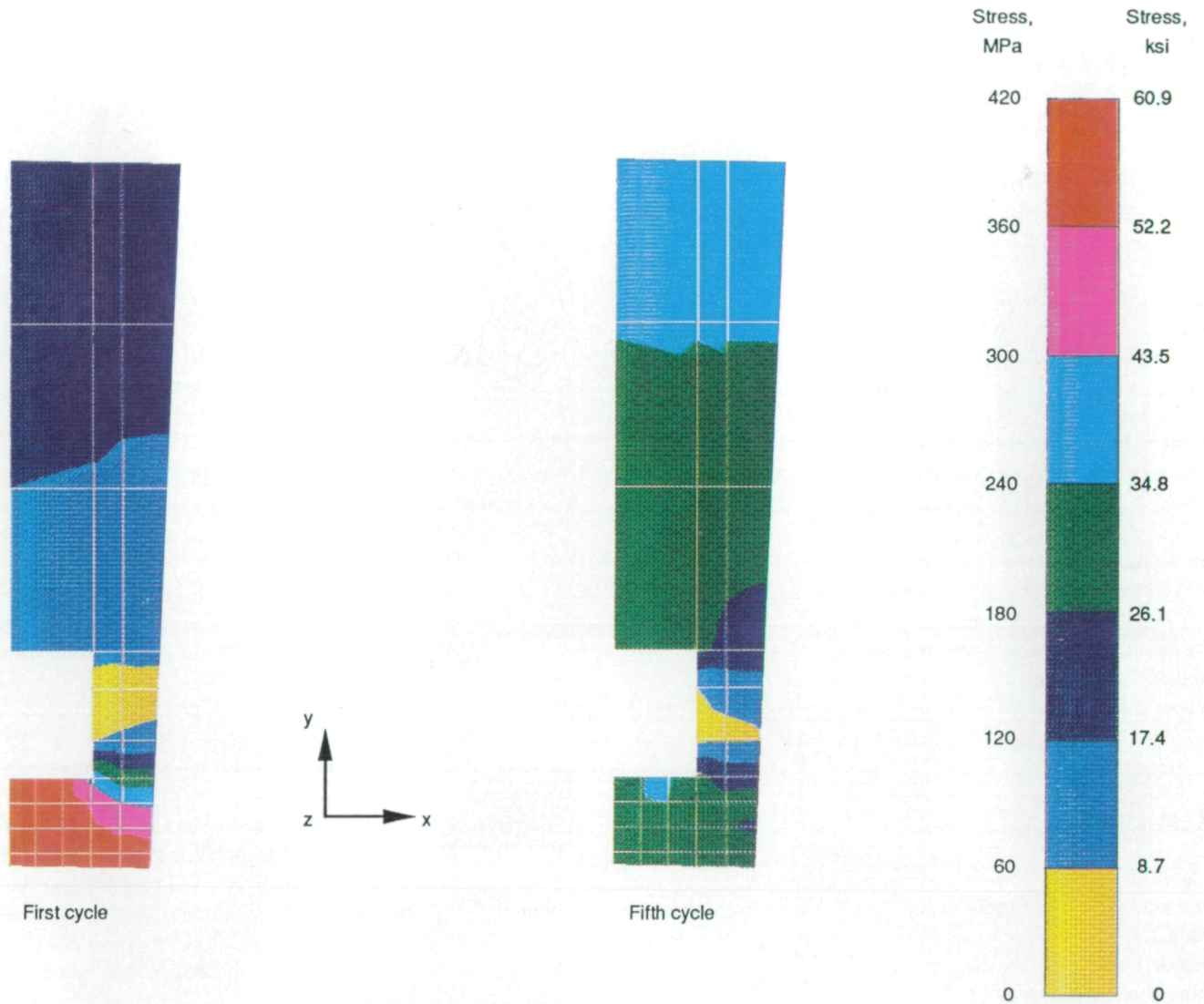
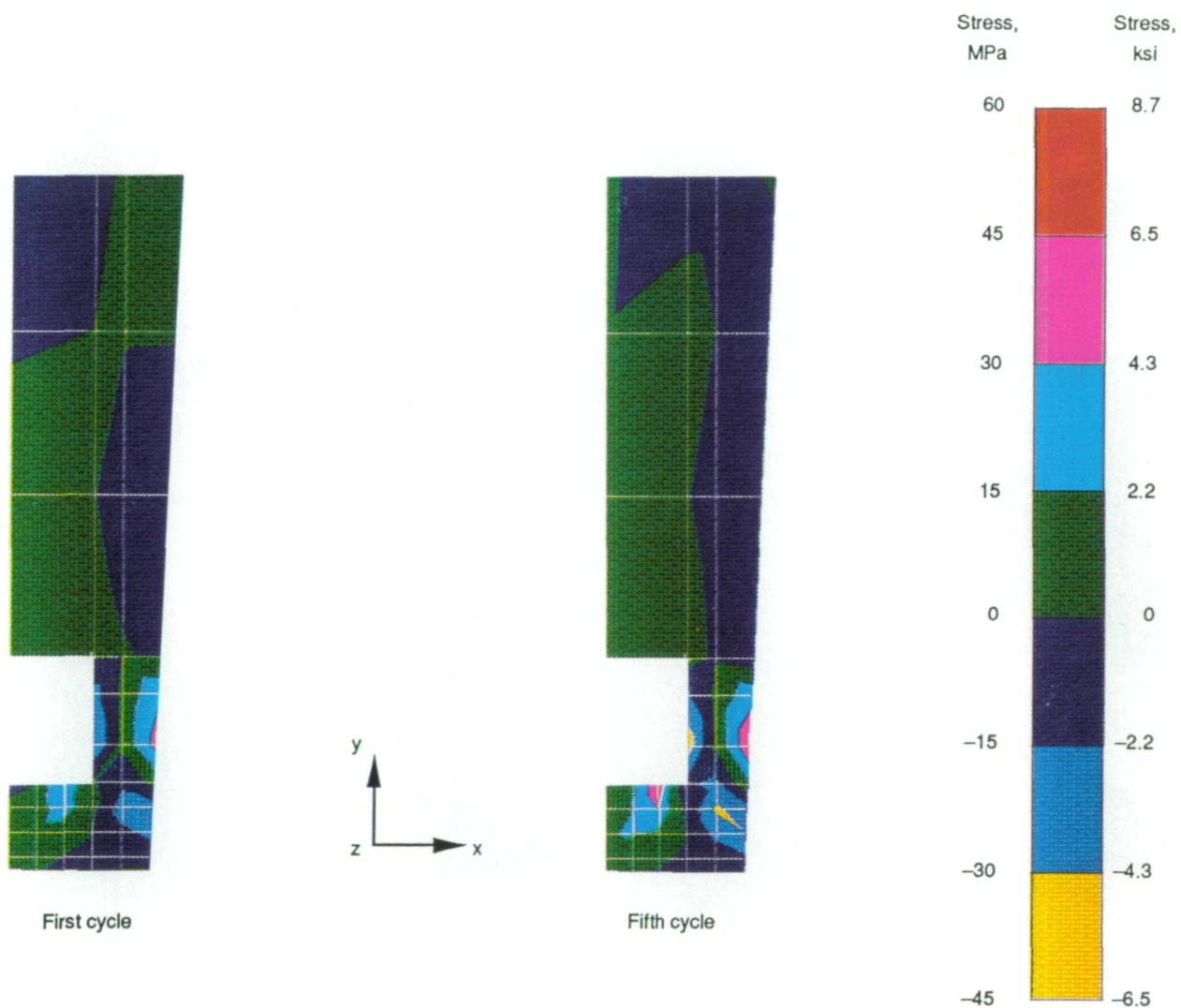Figure 5.—Stress distribution after different loading cycles; x-direction.

First cycle

Fifth cycle

7

First cycle

Fifth cycle

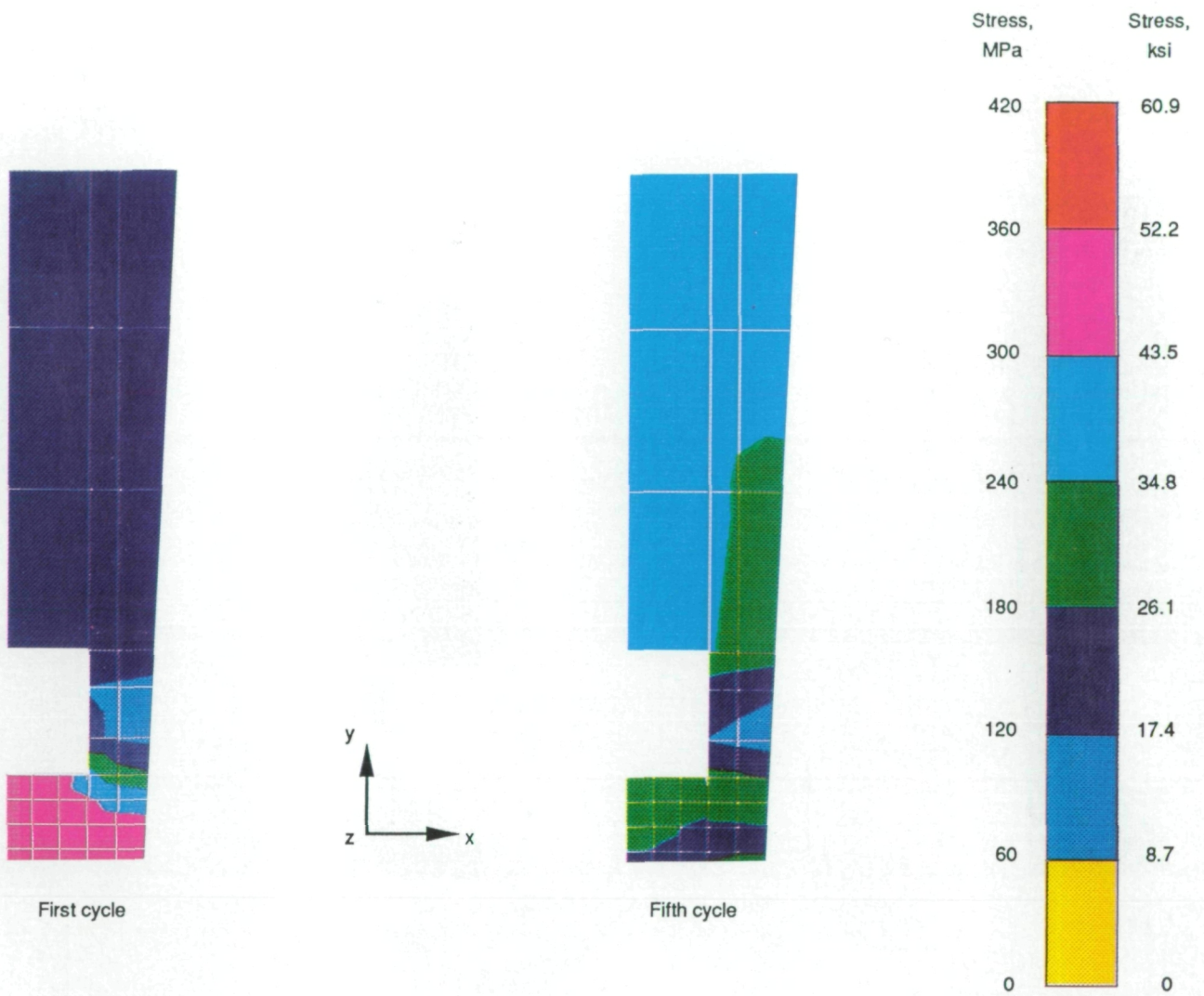Figure 6.—Stress distribution after different loading cycles; y-direction.

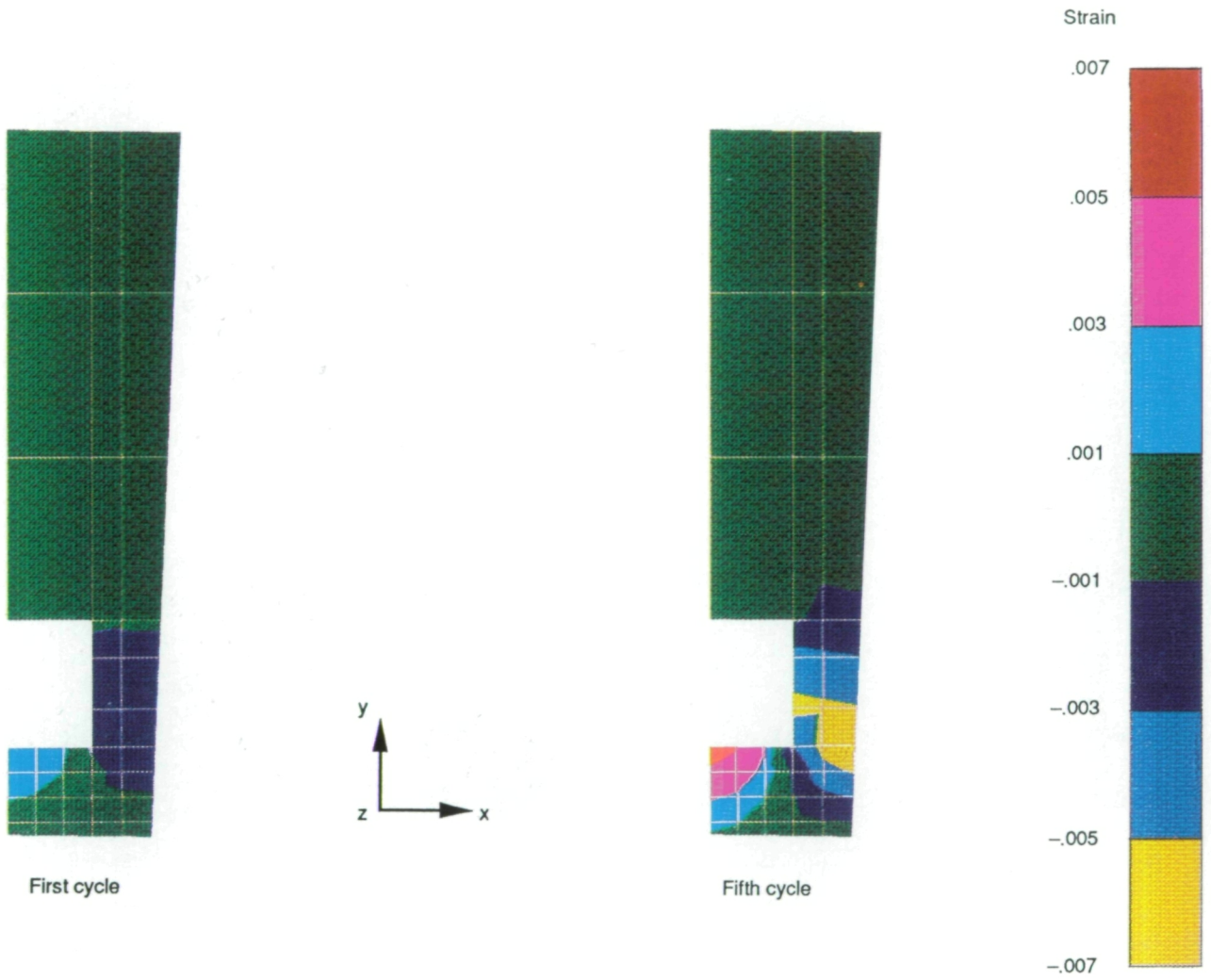Figure 7.—Effective stress distribution after different loading cycles.

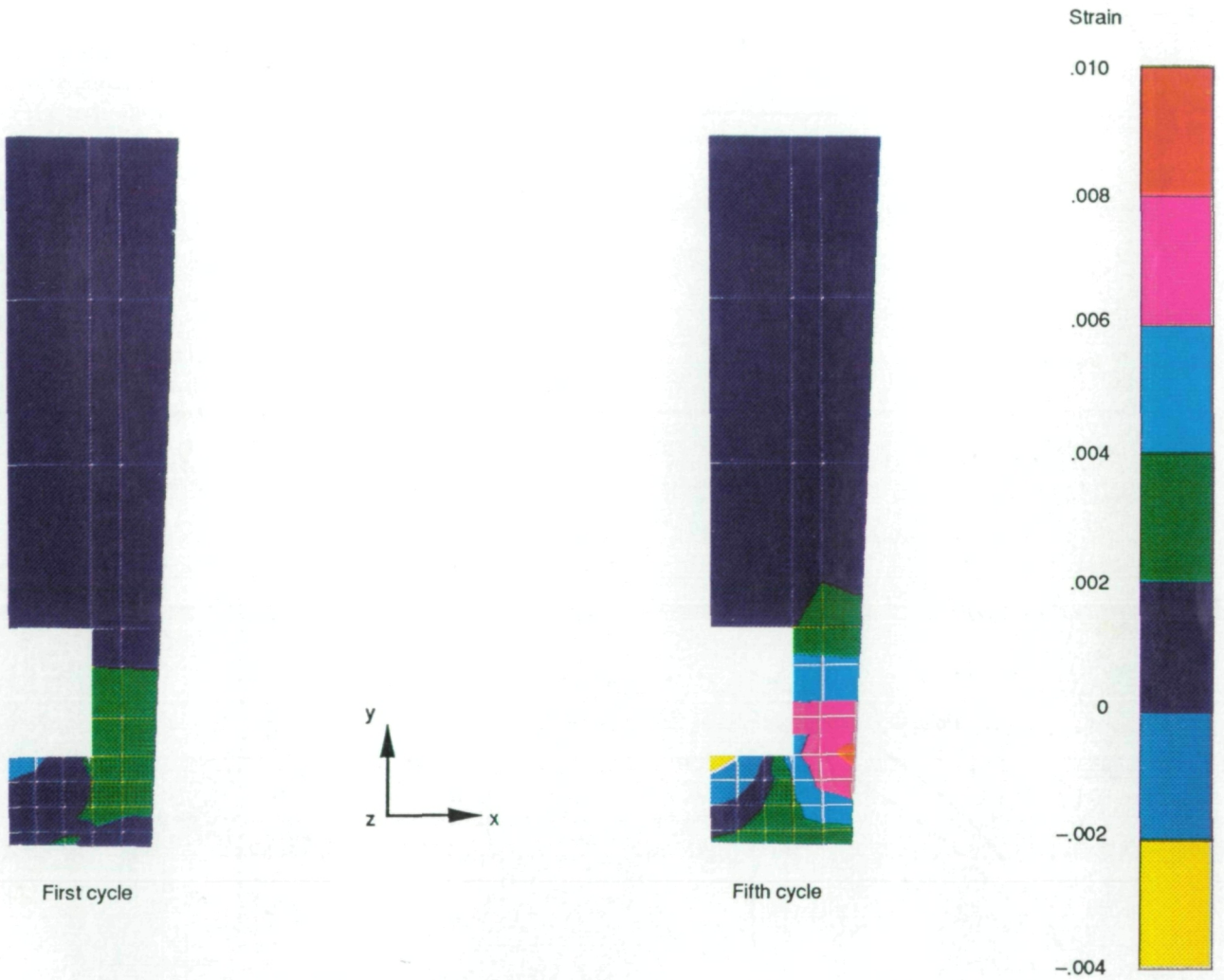Figure 8.—Strain distribution after different loading cycles; x-direction.

First cycle

Fifth cycle

Strain

.007

.005

.003

.001

−.001

−.003

−.005

−.007

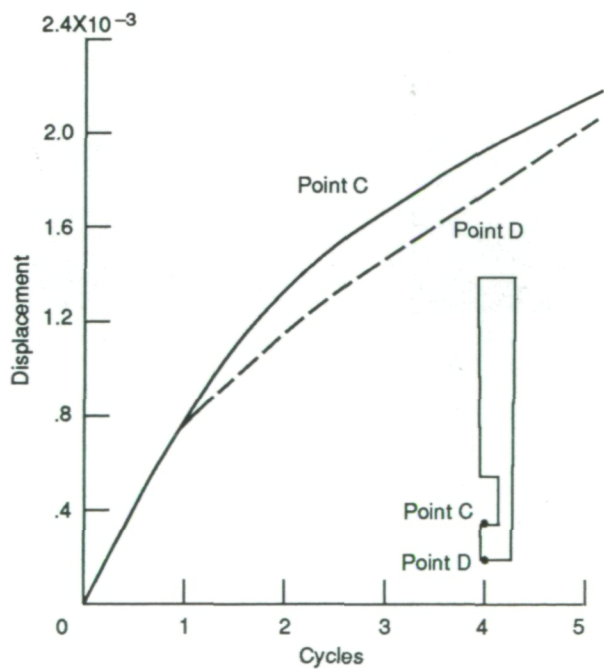Figure 9.—Strain distribution after different loading cycles; y-direction.

11
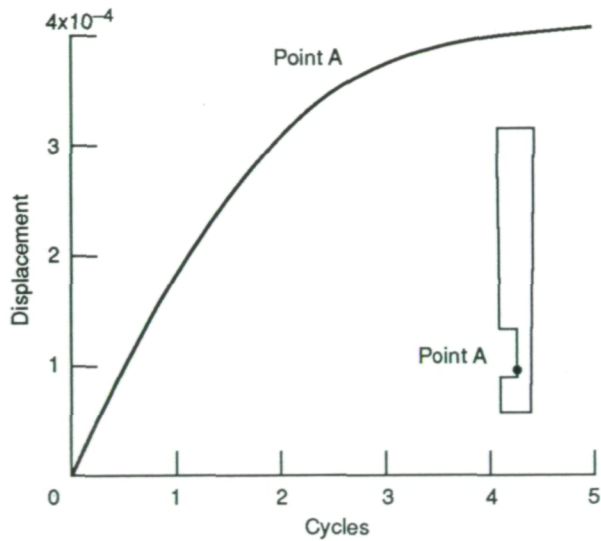
Figure 10.—Displacement in x-direction at a critical location on the cylindrical nozzle.

It is interesting to note that as the channel wall thins at the left end of the segment (see fig. 12), the material flows towards the right end and accumulates there. This is clear from figure 12 by comparing, at the right end, the original wall thickness of the segment (dashed lines) with the corresponding wall thickness after the fifth cycle (solid lines). The comparison shows an increase in the wall thickness at the right end of the segment.

Figure 13 shows the progressively deformed shape of the nozzle after the end of the first, third, and fifth cycles. The solid lines in the figure depict the shapes predicted by the viscoplastic analysis, and the broken lines show the shapes obtained from symmetry considerations. For ease of visual interpretation, a magnification factor of about 50 was employed for the predicted shapes. For a qualitative comparison, the shape of the segment observed in experiments after 393 cycles is also shown in this figure. The analysis qualitatively replicates the deformed shape of the segment observed in experiments.

A nonlinear elastoplastic analysis for these same thrust chambers was performed by Armstrong (ref. 3). The author was able to predict the progressively deformed shape and thinning of the coolant channel wall as a function of loading cycles. The deformed shape of the segment as predicted by this analysis is shown in figure 14. A comparison of figures 13 and 14 shows that the predicted shape from the current analysis resembles the observed shape more closely than that predicted in the reference 3 analysis.
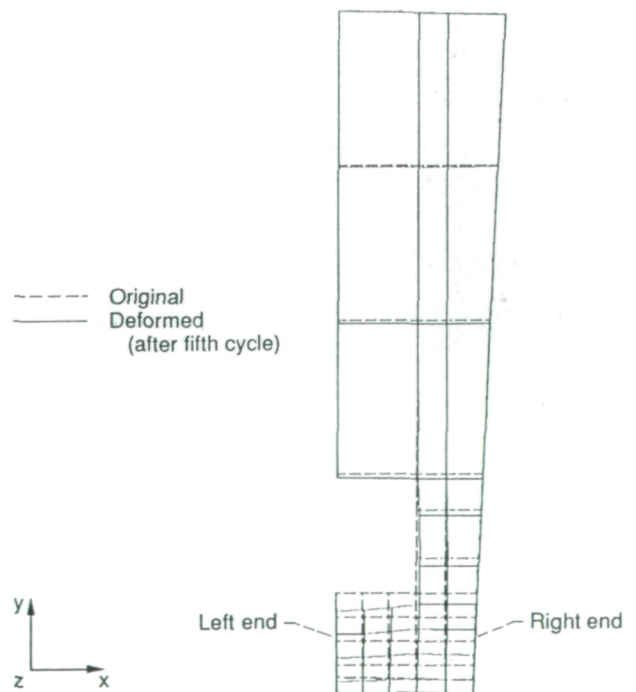

Figure 11.—Displacement (negative values) in y-direction at critical locations on the cylindrical nozzle.

Figure 12.—Original shape of the component and deformation after the fifth cycle.

Predicted from viscoplastic analysis
Obtained from symmetry considerations

Predicted shape after 1st cycle

Predicted shape after 3rd cycle

Predicted shape after 5th cycle
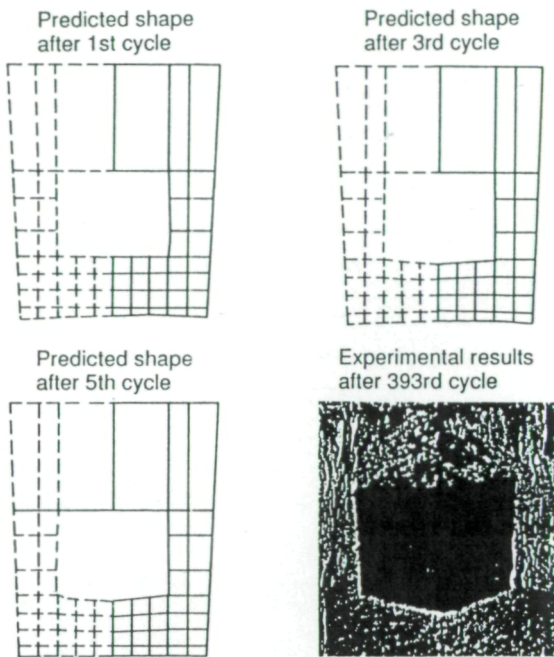
Experimental results after 393rd cycle

Figure 13.—Predicted and experimental shapes of the smallest repeating segment (experimental data from ref. 2).

Figure 14.—Predicted shape of the smallest repeating segment after 200 cycles (data from ref. 3).

Conclusions

A finite element stress-strain analysis for an experimental cylindrical thrust chamber was performed. An advanced viscoplastic model developed by Freed was employed to compute the time-dependent, inelastic strains in the nozzle. The thermal and mechanical loading cycles of the experiments were used to perform a nonlinear thermostructural analysis. The results show that the viscoplastic structural analysis qualitatively predicts the deformed shape and thinning of the component wall observed in experiments. It can therefore be concluded that the advanced viscoplastic models may be successfully employed to perform the realistic, nonlinear structural analyses of components subjected to complex thermomechanical loadings. Such analyses are required to assess the useful service life of these components. It is believed that the results from the present work will encourage other researchers and designers to employ the viscoplastic models for nonlinear inelastic analyses and thus for accurate estimates of the cyclic life of structural components.

References

1. Quentmeyer, R.J.: Thrust Chamber Thermal Barrier Coating Techniques. NASA TM–100933, 1988.
2. Quentmeyer, R.J.: Experimental Fatigue Life Investigation of Cylindrical Thrust Chambers. NASA TM X–73665, 1977.
3. Armstrong, M.H.: Structural Analysis of Cylindrical Thrust Chambers—Final Report. Vol. 1. NASA CR–159522, 1979.
4. Freed, A.D.; and Verrilli, M.J.: A Viscoplastic Theory Applied to Copper. NASA TM–100831, 1988.
5. Smith, J.P.: Systems Improved Numerical Differencing Analyzer (SINDA): User's Manual. NASA CR–134271, 1971.
6. MARC General Purpose Finite Element Program. Marc Analysis Research Corporation, Palo Alto, CA, 1983.
7. Arya, V.K.; and Kaufman, A.: Finite Element Implementation of Robinson's Viscoplastic Model and Its Application to Some Uniaxial and Multiaxial Problems. Eng. Comput., vol. 6, no. 3, Sept. 1989, pp. 537–547.
8. Arya, V.K.: Analytical and Finite Element Solutions of Some Problems Using a Viscoplastic Model. Comput. Struct., vol. 33, no. 4, Nov. 1989, pp. 957–967.
9. Arya, V.K.; Hornberger, K.; and Stamm, H.: On the Numerical Integration of Viscoplastic Models. Report No. KfK–4082, 1986.
10. Arya, V.K.: Finite Element Analysis of Structural Components Using Viscoplastic Models With Application to a Cowl Lip Problem. NASA CR–185189, 1990.
11. Arya, V.K.: Application of Finite-Element-Based Solution Technologies for Viscoplastic Structural Analyses. NASA CR–185196, 1990.

NASA	Report Documentation Page	
National Aeronautics and Space Administration		

1. Report No. NASA CR-185253	2. Government Accession No.	3. Recipient's Catalog No.

4. Title and Subtitle Nonlinear Structural Analysis of Cylindrical Thrust Chambers Using Viscoplastic Models		5. Report Date January 1991
		6. Performing Organization Code

7. Author(s) Vinod K. Arya	8. Performing Organization Report No. None (E-5512)
	10. Work Unit No. 553-13-00
9. Performing Organization Name and Address University of Toledo Toledo, Ohio 43606	11. Contract or Grant No. NCC3-120
	13. Type of Report and Period Covered Contractor Report Final
12. Sponsoring Agency Name and Address National Aeronautics and Space Administration Lewis Research Center Cleveland, Ohio 44135-3191	14. Sponsoring Agency Code

15. Supplementary Notes

16. Abstract

Elevated temperature and pressure levels are required for improving the performance of the Space Shuttle Main Engine (SSME). At these elevated temperatures, the thrust chamber of the engine experiences significant inelastic strains. For an accurate estimation of the life of the chambers and to predict their progressive deformation with the number of loading cycles, a realistic stress-strain analysis for the components must be made. This paper presents the results of a viscoplastic stress-strain analysis of a cylindrical thrust chamber used in experiments at the NASA Lewis Research Center. The experiments were designed to simulate the SSME operating conditions. The inelastic strain was calculated by using a viscoplastic model developed by Freed, and the quasi-three-dimensional structural analysis was performed by using the finite element program MARC. The temperatures and pressures were calculated by using the loading cycles of experiments, and these temperatures and pressures were used in the computations. The deformed shape of the component was predicted after the end of each loading cycle. The predicted shape qualitatively replicated the deformed shape of the component as observed in experiments. The results indicate that the use of viscoplastic models for structural analysis may lead to more realistic life assessments of experimental thrust chambers than achieved by other models.

17. Key Words (Suggested by Author(s)) Finite element analysis Viscoplasticity Nonlinear structural analysis Space Shuttle Main Engine	18. Distribution Statement Unclassified – Unlimited Subject Category 39		
19. Security Classif. (of this report) Unclassified	20. Security Classif. (of this page) Unclassified	21. No. of pages 15	22. Price* A03

National Aeronautics and
Space Administration

Lewis Research Center
Cleveland, Ohio 44135

FOURTH CLASS MAIL

ADDRESS CORRECTION REQUESTED

NASA